Effect of processing conditions on the bonding quality of FDM polymer filaments

Q. Sun
Jacobs Canada Inc., Calgary, Canada

G.M. Rizvi
Faculty of Engineering and Applied Science, University of Ontario Institute of Technology, Oshawa, Canada, and

C.T. Bellehumeur and P. Gu
Schulich School of Engineering, University of Calgary, Calgary, Canada

Abstract

Purpose – The purpose of this paper is to investigate the mechanisms controlling the bond formation among extruded polymer filaments in the fused deposition modeling (FDM) process. The bonding phenomenon is thermally driven and ultimately determines the integrity and mechanical properties of the resultant prototypes.

Design/methodology/approach – The bond quality was assessed through measuring and analyzing changes in the mesostructure and the degree of healing achieved at the interfaces between the adjoining polymer filaments. Experimental measurements of the temperature profiles were carried out for specimens produced under different processing conditions, and the effects on mesostructures and mechanical properties were observed. Parallel to the experimental work, predictions of the degree of bonding achieved during the filament deposition process were made based on the thermal analysis of extruded polymer filaments.

Findings – Experimental results showed that the fabrication strategy, the envelope temperature and variations in the convection coefficient had strong effects on the cooling temperature profile, as well as on the mesostructure and overall quality of the bond strength between filaments. The sintering phenomenon was found to have a significant effect on bond formation, but only for the very short duration when the filament's temperature was above the critical sintering temperature. Otherwise, creep deformation was found to dominate changes in the mesostructure.

Originality/value – This study provides valuable information about the effect of deposition strategies and processing conditions on the mesostructure and local mechanical properties within FDM prototypes. It also brings a better understanding of phenomena controlling the integrity of FDM products. Such knowledge is essential for manufacturing functional parts and diversifying the range of application of this process. The findings are particularly relevant to work conducted on modeling of the process and for the formulation of materials new to the FDM process.

Keywords Bonding, Thermal testing, Sintering, Creep

Paper type Research paper

Introduction

Fused deposition modeling (FDM) is a rapid prototyping technology suited for producing parts with complex geometries. The FDM machine is basically a computer numerically controlled gantry machine, carrying two miniature extruder head nozzles, one for the modeling material and the other for the support material. In the FDM process, parts are fabricated by extruding a molten filament through a heated nozzle in a prescribed pattern onto a platform (Figure 1). As the material is deposited, it cools, solidifies and bonds with the adjoining material. When one whole layer is deposited, the base plate moves down by an increment equal to the height of the filament and the next layer is deposited. FDM prototypes can be viewed as composites structures composed of partially bonded filaments. The process requires minimal manpower and is increasingly used to fabricate customized products for engineering as well as medical applications.

A key feature of the FDM process is its potential to fabricate parts with locally controlled properties (porosity, density and mechanical properties) (Li *et al.*, 2002). With continuing advances in materials and technology, it is even becoming possible to manufacture functional parts in addition to prototypes. In order for FDM to fully evolve into a manufacturing tool rather than just a prototyping tool, a number of improvements are essential:

- the mechanical properties of the parts produced should be enhanced so that they can maintain their integrity during service;

The current issue and full text archive of this journal is available at **www.emeraldinsight.com/1355-2546.htm**

Rapid Prototyping Journal
14/2 (2008) 72–80

[DOI 10.1108/13552540810862028]

The financial support for this work was provided by the Natural Sciences and Engineering Research Council of Canada (NSERC) through research grants awarded to Drs Bellehumeur and Gu. The authors also want to acknowledge the help that Mr Wen Lin and Ms Vanessa Millar have provided with the collection of experimental data.

Received: 31 October 2005
Revised: 1 October 2007
Accepted: 11 October 2007

Figure 1 Schematic of the FDM 2000 extrusion head and filament deposition process

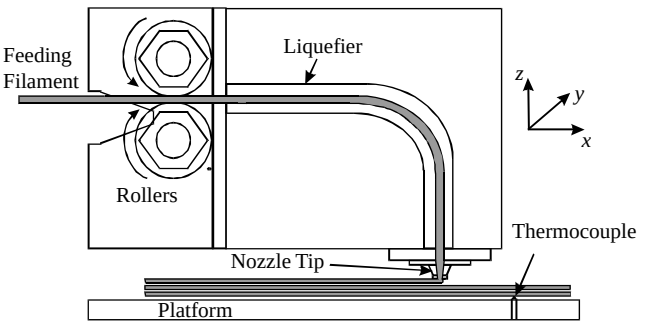

- the variety of polymeric materials available for use in these technologies should increase;
- the process improvements should result in greater dimensional control and better tolerances; and
- functional parts require improvements in surface finish.

To improve this promising technology, recent years have seen a substantial amount of research in the area of FDM manufacturing process planning. Research work has included the consideration of processing parameters in optimizing processing time (Comb *et al.*, 1994; Allen and Dutta, 1998; Alexander and Dutta, 2000; Han *et al.*, 2003), mechanical properties (Yardimci *et al.*, 1996; Yardimci, 1999; Rodríguez-Matas, 1999; Rodríguez *et al.*, 2001; Bellini, 2002; Sung *et al.*, 2002) and surface accuracy of the final product (Anitha *et al.*, 2001; Luis Perez, 2002; Pandey *et al.*, 2003). Few models have been proposed (Li *et al.*, 2002, 2003; Kulkarni and Dutta, 1999; Rodríguez *et al.*, 2003) that show promise in terms of their predictive value. The common drawback of models currently available in the literature is that their domain of validity is greatly limited, for they either neglected the partial bonding between filaments or relied heavily on the empirical determination of fitting parameters. Effort has also been invested into the formulation and processing of polymeric materials new to the FDM process (Gray *et al.*, 1998; Zhong *et al.*, 2001; Kalita *et al.*, 2003; Shofner *et al.*, 2003; Wang *et al.*, 2003). Limited success was achieved in the production of a durable and satisfactory end product. Most studies showed that the mechanical properties of the parts were negatively influenced by the insufficient bond strength achieved between filaments, the weak interlayer strength in the building direction often being the weakest and most critical link in the FDM parts.

The formation of bonds among polymer filaments in FDM parts is driven by the thermal energy of the extruded material. The temperature history of interfaces plays an important role in determining the bonding quality and therefore the mechanical properties of the final product. The bonding quality depends on the growth of the neck formed between the adjacent filaments and on the molecular diffusion and randomization of the polymer chains across the interface (Figure 2). In this work, the term healing refers to the molecular diffusion at the interface between filaments while sintering is used to describe the neck growth phenomenon driven by surface tension. Early studies on sintering dealt mostly with metals and ceramics and showed that the process is dominated by volume, surface and grain boundary diffusion. For polymeric materials, sintering is due mostly to the viscous flow mechanism (Narkis, 1979;

Figure 2 Bond formation process between two filaments: (1) surface contacting; (2) neck growth; (3) molecular diffusion at interface and randomization

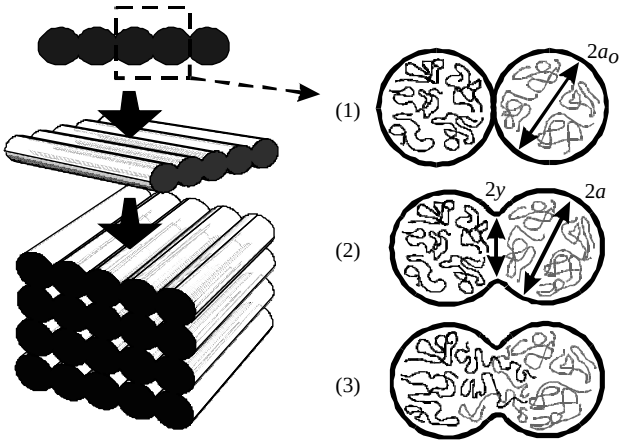

Rosenzweig and Narkis, 1981; Bellehumeur *et al.*, 1996). While the term is normally used to describe coalescence occurring below the melting point of the material, the expression has been carried on and accepted in the literature for the coalescence of polymers above their glass and melting transitions.

It was felt that there is a scarcity of data on the mechanism of bond formation between adjacent filaments making up FDM parts. Therefore, considerable research effort is still needed to fully understand the effects of material and processing parameters on the mechanical properties of the parts fabricated. In particular, there is next to no literature on the experimental determination of the thermal profiles of parts built using FDM. This data is especially important, as it is indicative of the bond formation between adjacent filaments and their influence on the mechanical properties. This paper provides the results of experimental determination of the thermal profiles of some simple shapes produced using the FDM process, their effects on the bond formation in terms of neck growth between adjacent filaments and the intermolecular diffusion at the interface, and their evaluation in regards to the mechanical properties of the parts.

Experimental work

The specimens used in this study were made on a Stratasys FDM 2000 using a commercial acrylonitrile butadiene styrene (ABS P400). The liquefier temperature was set at 270°C and the polymer filament was extruded through a nozzle onto a platform in "solid fine" mode. All parts were built using tip 12 (0.305 mm inner diameter). The size of the extruded filament was larger than the diameter of the tip due to swelling. The flow rate and vertical position of the head were adjusted to control the dimension of the deposited filament (0.254 mm in height and 0.508 mm in width). The envelope temperature was set to 70°C. The temperature settings used for the experiments were those recommended by the manufacturer. All parts produced in this study were made with unidirectional filaments, which is contrary to the normal practice of keeping the filaments of alternating layers perpendicular to each other to provide optimal strength. This was done in order to enhance the effects of the parameters being studied on the bonding between

adjoining filaments. The parts produced for mesostructure characterization and for mechanical testing were built with the normal five layers of support material. However, the parts made for the measurements of the temperature profiles were built without the support layers, as the support material may have had different thermal characteristics.

The temperature profiles of extruded filaments were monitored using 0.0118 mm K-type thermocouples. Measurements of the lower portion of the tip and of the filament as it exited the nozzle were performed. While the liquefier temperature was set to 270°C, all tests results showed that the tip temperature ranged from 258 to 260°C. Further measurements were conducted while the thermocouple remained imbedded in the foam of the base plate of the FDM 2000 machine and layers of filaments were deposited onto it (Figure 1). The measurements were recorded and analysed through a high-frequency analog-digital converter (1,000 readings per second), data acquisition card 6024E and Labview 6/7 software (National Instruments).

The quality of the bond achieved between filaments was evaluated based on the mesostructure characteristics and three-point bending tests results. The mesostructural feature of interest to our work was defined as the variation in the neck growth between adjacent filaments (Figure 3). Samples collected from the parts were sectioned using a Leica RM2165 microtome. The samples' cross-sections were viewed under an Olympus BX60 optical microscope. Pictures of these cross-sections were taken with a CCD camera mounted on the optical microscope, and the features were analyzed using the image analysis software Image-Pro®. The three-point bending tests of the specimens were carried out on Adelaide Testing Machine (Model TTS Series). There are no ASTM standards for testing filamentary plastic parts; therefore, tests conformed to ASTM standard D 1184-98 for flexural strength of laminated sheets bonded with glue. One deviation from the chosen standard was that failure occurred between filament bonds in the same layer rather than in the bonds between adjacent layers. The specimens were constructed so that all filaments were oriented perpendicular to the longitudinal axis of the parts so the test failure would occur in the bonds between adjacent filaments (Figure 4). The test also differed from the standard in that 12 layers of laminates were used instead of the stipulated eight layers, so that parts with reasonable dimensions could be tested.

To study the impact of the deposition strategy on the temperature history of the polymer filaments, two geometries were chosen for thermal and mesostructure studies. Rectangular parts were built while changing the orientation of the filament:

1 200 × 12 × 2.8 mm, in which the filaments were deposited in the longitudinal direction; and

Figure 3 Microphotograph of the cross-sectional area of a FDM part where *W* is the filament's width; *H* is the filament's height; 2*y* is the neck length between adjacent filaments

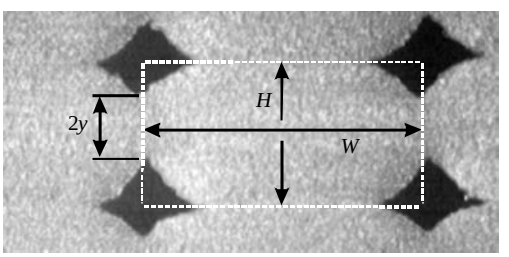

Figure 4 Schematic of bending test specimen

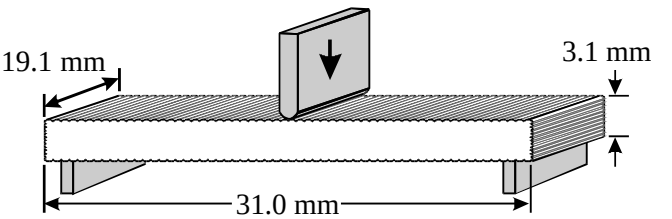

2 130 × 28 × 2.8 mm, in which the filaments were deposited in the lateral direction.

All other specimens were otherwise built to meet the specifications shown in Figure 4. The effects of changing the liquefier and envelope temperatures on the cooling characteristics, mesostructure and flexural strength of the FDM parts were investigated. Three envelope temperatures of 50, 60 and 70°C were chosen, as the FDM 2000 machine only allowed us to set envelope temperature below 72°C.

Results and discussions

Thermal processes in FDM and model validation

The temperature history of the filament is a critical parameter in dictating part strength. This temperature history depends upon the rate at which the filament cools upon leaving the extrusion head. Several heat transfer models describing the FDM process have been proposed in the literature. This section discusses models presented in the literature and assesses their validity with experimental data obtained when processing ABS P400.

Yardimci (1999), Yardimci and Guceri (1996) and Yardimci *et al.* (1996) developed a family of numerical models for the fused deposition ceramic process. A similar analysis is applicable to the FDM process that uses thermoplastic polymer as a raw material. Rodríguez-Matas, 1999 conducted a transient 2D analysis of the FDM process using a finite element method. Thomas and Rodríguez (2000) later presented a modified analysis of the process in which they idealizing the cross section of the filaments to be rectangular.

The analysis was applied to a filament being deposited on a vertical stack (Figure 5). They assumed a perfect contact among stacked filaments. For initial condition, the temperature at the interface immediately following the deposition of the filament, T_{ave}, was averaged between the envelope temperature (T_E) and the liquefier temperature (T_L), and finally the following

Figure 5 Schematic of the deposition and cooling of a filament in the FDM process: (a) rectangular geometry used in 2D analytical model proposed by Thomas and Rodríguez (2000); (b) geometry used in LC analytical model proposed by Li *et al.* (2003)

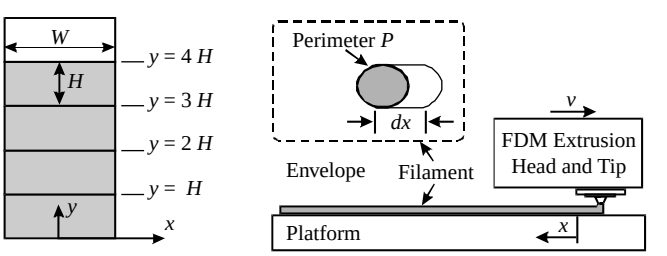

analytical solution was obtained (Thomas and Rodríguez, 2000):

$$T_{\text{ave}}(x,y,t) = T_{\text{E}}\left[1+\sum_{m=1}^{\infty}\sum_{n=1}^{\infty}(a_{mn}\sin(\lambda_m y)\cos(\beta_n x))\mathrm{e}^{-\alpha^2\left(\lambda_m^2+\beta_m^2\right)t}\right] \quad (1)$$

where:

$$a_{mn} = \frac{4T_{\text{L}}^*}{E_m^2F_n^2\lambda_m\beta_n}\sin\left(\frac{9\lambda_m H}{2}\right)\sin\left(\frac{\lambda_m H}{2}\right)\sin\left(\frac{\beta_n W}{2}\right) \quad (2)$$

$$E_m^2 = \frac{1}{2}\left(5H-\frac{\sin(10\lambda_m H)}{2\lambda_m}\right) \quad (3)$$

$$F_n^2 = \frac{1}{2}\left(w-\frac{\sin(\lambda_n\beta_n W)}{\beta_n}\right) \quad (4)$$

$$\alpha^2 = \frac{k}{C\rho} \quad (5)$$

where H, W are the filament's height and width, while t, C, k, and ρ represent the time, heat capacitance, thermal conductivity, and density, respectively. The eigenvalues λ_m and β_n are the roots of the following transcendental equations:

$$\lambda_m\cot(5\lambda_m H) = \frac{-h}{k}, \quad \beta_n\tan\left(\frac{\beta_n W}{2}\right) = \frac{h}{k}. \quad (6)$$

Results presented by Rodríguez showed that the temperature gradients along both the width and height of the filament rapidly become negligible following the deposition of the top layer filament. This result is not surprising considering the small size of the filament. On that basis, Li *et al.* (2003) used the lumped capacity (LC) analysis for modeling the cooling process of the extruded filament. In their analysis, the cooling process of a single filament was thus simplified into a one-dimensional transient heat transfer model, and the cross-sectional shape of the deposited filament was modeled as an ellipse (Figure 5). The analytical solution proposed by Li *et al.* (2003) is as follows:

$$T = T_{\text{E}} + (T_{\text{L}} - T_{\text{E}})\mathrm{e}^{-mx} \quad (7)$$

with:

$$m = \frac{\sqrt{1+4\alpha\beta}-1}{2\alpha} \quad \text{and} \quad x = vt \quad (8)$$

where:

$$\alpha = \frac{k}{\rho C v} \quad \text{and} \quad \beta = \frac{hP}{\rho C A v}, \quad (9)$$

The terms A, P and v represent the cross section area of the filament, the perimeter of the filament and its deposition velocity, respectively.

Heat transfer model validation

Experimental measurements performed on filaments deposited on the base plate foam platform were used to assess the validity of the two models described above. The temperature of the filament as it leaves the tip and is deposited onto the platform was found to range from 235 to 245°C, which is significantly lower than that specified for the liquefier (270°C) as well as that measured for the tip (260°C). The control system in the liquefier, the time gap in measurement and the response time of thermocouple are the most probable reasons to explain this difference.

Figure 6 shows a comparison between the theoretical model predictions and experimental data collected for the cooling profile of a single deposited filament. The Newton-Raphson technique was used to solve the eigenvalues of transcendental equations for the model presented by Thomas and Rodríguez. The material properties were selected based on the work presented by Li *et al.* (2003) and are summarized in Table I.

The measured data, in spite of the measurement limitations, are in general agreement with the two models considered in this work. The interface temperature rises above the glass transition temperature (T_{g}) immediately upon extrusion of the filament and stays above T_{g} only for a very short period of time.

Figure 6 Experimental profiles compared with model predictions

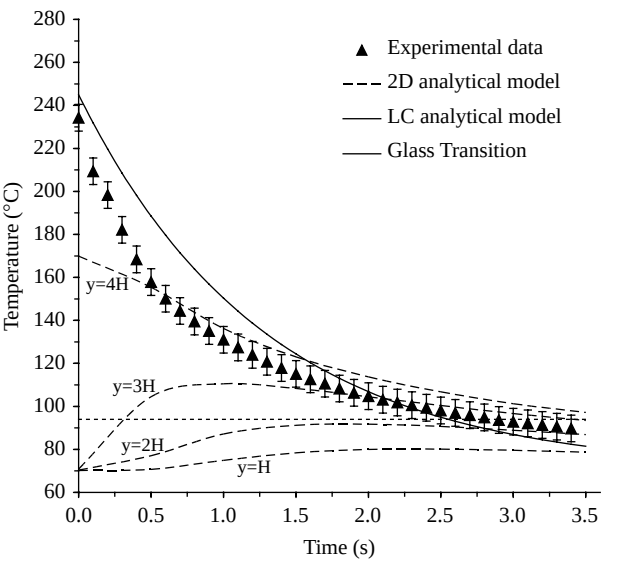

Notes: The solid line represents the LC analytical model (Li *et al.*, 2003) with initial temperature of 245°C and $h = 140$ W/m^{2}K. The dash lines represent the 2D analytical model predictions at various height for a stack of five filaments (Thomas and Rodríguez, 2000) with $h = 75$ W/m^{2}K. The terms y and H are the vertical position and the filament's height, respectively

Table I Material properties of ABS P400

Parameter	Values	Reference
Thermal conductivity k (W/m K)	0.177	Rodríguez-Matas (1999)
Specific heat C_p (J/kg K)	2,080	Rodríguez-Matas (1999)
Density ρ (kg/m^3)	1,050	Rodríguez-Matas (1999)
Glass transition temperature T_g (°C)	94	Rodríguez-Matas (1999)
Viscosity μ at 240°C (Pa s)	5,100	Sun (2005)
Model parameter b in $\mu = 5,100\exp[-b(T-503)]$ with T (K)	0.056	Sun (2005)
Surface tension Γ at 240°C (N/m)	0.029	Sun (2005)
Temperature dependence: $\Delta\Gamma/\Delta T$ (N/m K)	-3.45×10^{-4}	Sun (2005)

It is interesting to note that at the higher temperatures prevailing in the initial stage, the measured temperature profile exhibits more similarity to the LC model predictions (Li *et al.*, 2003), due to enhanced radiation and convection at higher temperatures. On the other hand, at lower temperatures the measured data tend to follow the 2D model predictions (Thomas and Rodríguez, 2000).

Changes in the temperature profile of a deposited filament during the fabrication of parts with multiple layers have been determined. Preliminary results were obtained for 38 by 38 mm specimens having a thickness of 15 as well as 30 layers of filaments. The thermocouple was positioned in the center of the square cross-section area of the specimens, and the results are shown in Figure 7. The temperature profiles obtained for both the 15- and 30-layer specimens show that the temperature of the filament located on the bottom layer periodically rises above the glass transition temperature with the deposition of each additional layer to the specimen. Each peak was followed by a rapid decrease in the temperature as the extrusion head moved away from the center position of the specimen. The minimum temperature (lower limit), increases with the number of layers deposited onto the platform. The profiles shown in Figure 7 show that the filaments remain above the glass transition temperature during a significant portion of the fabrication process. This confirms the importance of heat transfer through conduction within the structure with the deposition of the filament, as suggested from the predictions obtained using the 2D analytical model proposed by Thomas and Rodríguez (2000) (Figure 6). Experiments and model predictions suggest that the heat transferred through conduction from the top layered filament affect the development of bonds between lower layers of filaments.

Neck growth mechanisms and model validation

The temperature profiles described in the last section show that the bottom layers of the parts remain at temperatures higher than T_g for a longer period of time than the upper layers. The neck growth between adjacent filaments of the same layer is expected to be larger in the bottom layers than in the top layers.

Figure 7 Temperature profile of the bottom filament for a 38 × 38 mm × 15-layer part and a 38 × 38 mm × 30-layer part

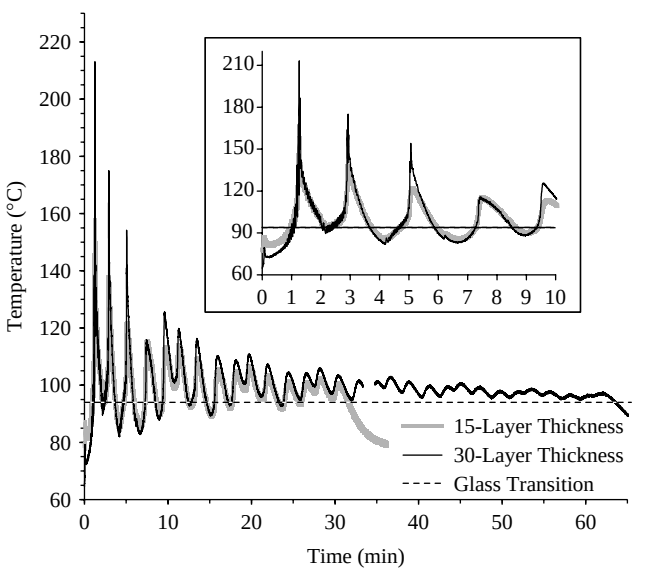

This phenomenon is more apparent in the 30-layer specimens (Figure 8). The voids in the lower region are clearly smaller than in the upper region, indicating larger neck growth in the bottom regions of the part.

The experimental results obtained for the dimensionless neck radius achieved between adjacent filaments were compared to the predictions obtained from a Newtonian sintering model proposed by Pokluda *et al.* (1997) following an approach presented by Bellehumeur *et al.* (2004).

$$\frac{d\theta}{dt} = \frac{\Gamma}{a_0 \mu} \frac{2^{5/3}\cos(\theta)\sin(\theta)(2-\cos(\theta))^{1/3}}{(1-\cos(\theta))(1+\cos(\theta))^{1/3}} \quad (10)$$

The term $\theta = \sin^{-1}(y/a)$ while a_0, μ, and Γ represent the initial particle radius, the viscosity, and the surface tension, respectively. The Newtonian sintering model was combined with the predictions obtained from the LC heat transfer model proposed by Li *et al.* (2003). The polymer viscosity of ABS P400 was determined from measurements performed using a HAAKE RS150 rheometer and reported to be 48,000, 14,000 and 5,100 Pa s at temperatures of 200, 220 and 240°C, respectively. The surface tension of the ABS P400 was estimated based on results obtained from isothermal and non-isothermal sintering experiments, as described by Bellehumeur *et al.* (2004). The temperature dependence of the material viscosity and surface tension were taken into consideration in the sintering model, while the thermal properties (heat capacitance, thermal conductivity, and density) were assumed to be constant in the heat transfer model.

Table II summarizes experimental results and model predictions describing the neck growth between adjacent filaments under conditions used to produced the 38 × 38 × 30-layers part. The dimensionless quantity y/a represents the ratio between the neck radius and the filament's radius. Note that in the

Figure 8 Microphotograph of the cross-sectional area of a 38 × 38 mm × 30-layer part

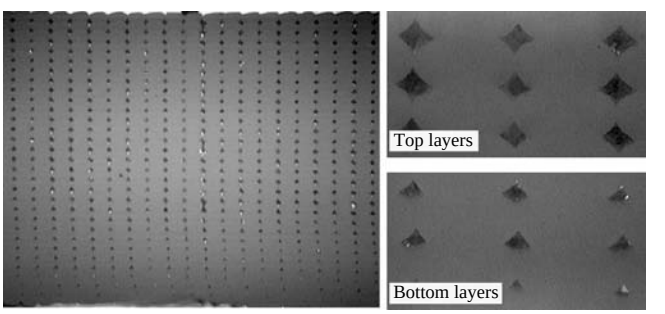

Table II Dimensionless Neck Radii in a 30-layer part

	Experimental results		Model predictions T_L = 270°C, T_E = 70°C < br > h = 140 W/m^2 K
	Bottom layers[a]	Top layers[a]	
Neck radius y (μm)	75.4	50.9	32.9
Standard deviation (μm)	2.63	2.69	–
Dimensionless neck radius (y/a)	0.61	0.41	0.14

Note: [a]Measurements performed on 4 layers

sintering model prediction, the radius of the filament is equivalent to that of an ideal circle: 0.235 mm. In real experiments, the particle radius is assumed to be the minor radius of the ellipse, which is only 0.123 ± 0.0025 mm. The theoretical model greatly underestimated the neck growth achieved between adjacent filaments. Moreover, experimental results showed that the dimensionless neck growth in the top few layers was significantly smaller compared to that measured near the bottom layers (Table II).

Experimental observation reported by Bellehumeur *et al.* (2004) for the sintering of ABS P400 suggested that most of the neck growth occur when the temperature of the filament was above the critical sintering temperature (200°C for ABS P400). The temperature profiles shown in Figure 7 show that this condition is met only during the first few seconds following the deposition of the filament onto the platform. Variations in the neck growth with the vertical position are due to the exposure of the material to temperatures above the glass transition while below the critical sintering temperature. The differences between the model predictions and experimental observations cannot be attributed to sintering and are likely due to creep deformation under the effect of gravity or the continued downward pressure from the FDM head while the part is being built.

Effects of filament deposition strategy

When 3D parts are being built, the temperature within different regions of the part changes according to the motion of the FDM extrusion head since it is at a much higher temperature than the envelope region. Therefore, it is expected that both the part geometry and the motion pattern followed by the extrusion head influence the cooling rate of the part underneath it. This, in turn, should affect the bond strength between adjacent filaments. Figure 9 shows the temperature profiles at about the center of the base of parts for which the filaments were deposited in the longitudinal and lateral directions. The secondary peak which periodically appears in the temperature profile coincides with the completion of each layer. At that point, the extrusion head moves past the center of the part as it is moved towards the starting point for the deposition of a new layer. For the longitudinally built part, the temperature at the base remains above T_g for most of the build time. The peak temperatures remain relatively low since the hot extrusion tip moves quickly past any building region at the center, traveling a long distance away and allowing the filaments to cool down before the tip re-approaches this region again. For the laterally built part, due to the short path length, the hot tip spends a long continuous period of time near any building region. For each pass, the peak temperatures reaches higher values as the FDM head approaches the thermocouple; and, the temperature of the deposited layer dropped to values below the T_g limit as the hot tip moves away. Overall, the average building temperature for the laterally built part (112.2°C) is higher than that for the longitudinally built part (99.9°C).

Figure 9 Effect of deposition strategy (orientation of filaments) on the cooling temperature profile

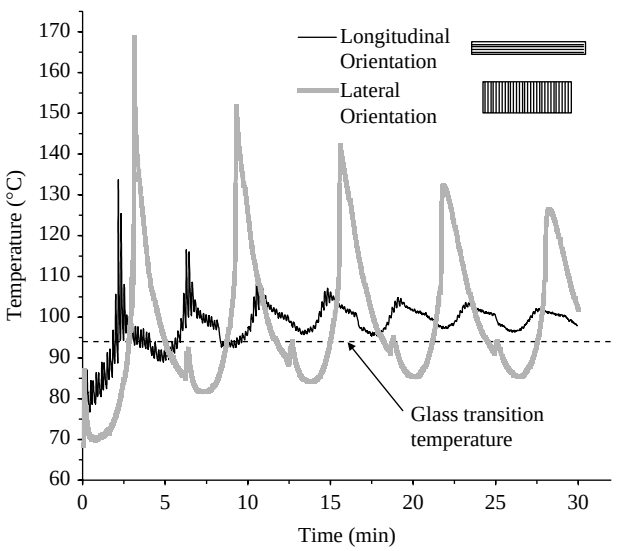

Table III summarizes the results obtained for the dimensionless neck formed between adjacent filaments. The neck radius values represent an average of measurements performed in the middle-layer of the part. Furthermore, the measurements were taken only in the middle of the cross-section to eliminate the edge effect. The specimens built with filaments-oriented laterally exhibit higher dimensionless neck radius and lower porosity compared to the ones with the filaments-oriented longitudinally. This result is consistent with our observations reported for the temperature profiles of deposited filaments (Figure 9).

Effects of other processing parameters

Figures 10 and 11 show the temperature profiles recorded while varying the liquefier and envelope temperatures. Increasing the envelope temperature has an important effect on raising the lower limit in the temperature profile of the deposited filament. For comparison purpose, we have defined T_{MIN} as the average of the lowest temperature reached at each deposition pass. T_{MIN} at envelope temperatures of 50, 60 and 70°C are 73, 80 and 87°C, respectively. On the other hand, increasing the liquefier temperature from 260 to 280°C did not show any significant effect on the temperature of the deposited filaments.

Attempts were made to evaluate the effect of liquefier and envelope temperatures on the bond strength achieved between filaments. In the FDM process, the filament's temperature remains above the glass transition for a relatively long period of time. Under such conditions, the intermolecular diffusion occurring across interfaces, often referred to as healing, is an important mechanism to consider. The interface between filaments gradually disappears and mechanical strength at the interface develops. In the bulk amorphous polymeric material, the motion of a chain is greatly restricted by the entanglement of neighbouring chains.

Table III Effect of building strategy on the mesostructure

	Filament orientation	
	Longitudinal direction	Lateral direction
Neck radius y (μm)	45.4	55.4
Standard deviation (μm)	4.2	2.9
Dimensionless neck radius (y/a)	0.37	0.45
Average building temperature (°C)	99.9	112.2

Figure 10 (a) Temperature profiles at various liquefier temperatures (envelope temperature: 70°C) and (b) temperature profiles at various envelope temperatures (liquefier temperature: 270°C)

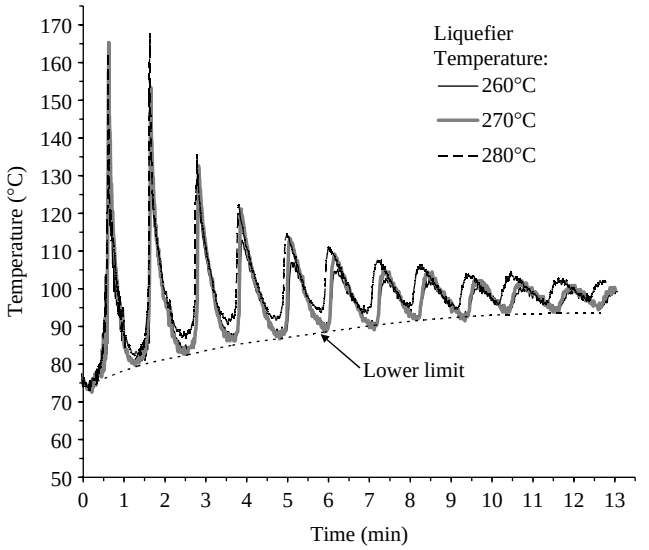

Figure 11 (a) Temperature profiles at various liquefier temperatures (envelope temperature: 70°C) and (b) temperature profiles at various envelope temperatures (liquefier temperature: 270°C)

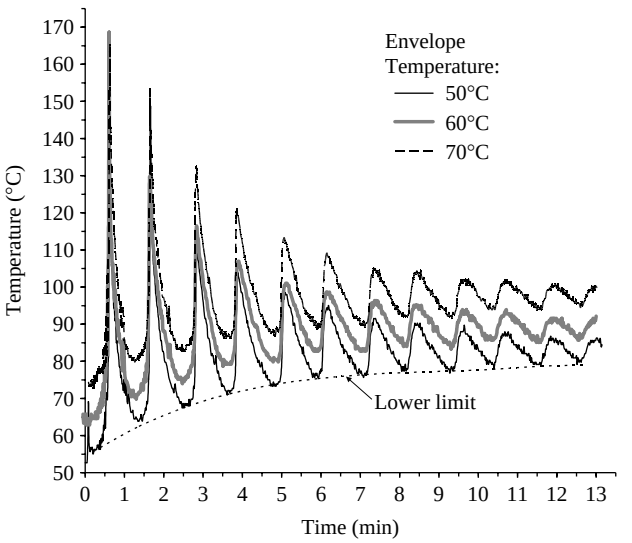

A relationship between the mechanical properties of a healed interface with temperature and contact time can be defined based on the so-called healing theory (De Gennes, 1971; Wool, 1995). While several studies have been devoted to this topic, model predictions should be used with caution as they are very sensitive to changes in the temperature and estimated values for model parameters. Alternatively, the mechanical strength is a property that is most sensitive to changes in the degree of healing achieved at an interface.

In this work, the quality of bond achieved between adjacent filaments during the fabrication process is assessed based on the three-point bending test results. Changes in the mesostructure, from sintering and creep deformation, also influences the testing results. Nevertheless, the bending test provides partial information on the extent of intermolecular diffusion realized under different processing conditions. A minimum of ten replicates were generated for each processing condition. To facilitate the timely completion of the tests, 24 specimens were built simultaneously on the FDM platform (Figure 12). The orientation of the filaments and dimensions of the test specimens are shown in Figure 4. Analysis of failure data showed a large standard deviation and effects considered were non-significant. Similarly, variations in the liquefier or envelope temperatures did not result in any significant difference in the parts' mesostructures. On the other hand, we observed that parts in a certain location consistently had a better surface appearance (smooth surface with no fault lines between adjacent filaments) compared to that of parts produced at different locations. The variability in experimental results was likely due to the variations in the cooling conditions with changing the building location. The effect of this processing parameter was further examined and the temperature profiles obtained with parts built at different locations on the platform were carried out. The temperature profiles greatly varied with changes in the building location. Such variations in the thermal history imposed on each of the parts are expected to have influenced both the mesostructure and the quality of the bonds formed between filaments. Figure 13 shows the temperature profiles at the base of the parts made at locations 1, 9 and 15. These three locations were selected as they represent best the highest, lowest and average temperature traces recorded in our experiments.

In the FDM 2000, the envelope temperature is controlled through heating and circulation of enclosed air. Our temperature measurement showed that the temperature distribution within the build envelope is adequately homogeneous. However, the air flow field within the building chamber was found to be far from homogeneous, which is consistent with observations reported by Yardimci (1999). The air flow field is sensitive to the building location on the platform and, thus, has a strong effect on the convection coefficient distributions on a part's surface. Variations in the failure load, as well as in the mesostructure characteristics for parts built at different locations, were quantified and results are presented in Table IV. The parts at location 9 exhibits a 31 percent larger neck growth than the parts made at location 1. Moreover, the creep deformations seen for parts at location 9 are larger than for parts at location 1. We attribute these differences to the fact

Figure 12 Location of parts built on the FDM 2000 platform (top view) for the parametric study

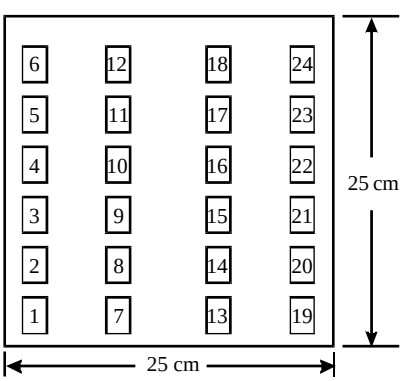

Figure 13 Variation in temperature profiles with varying the part building locations

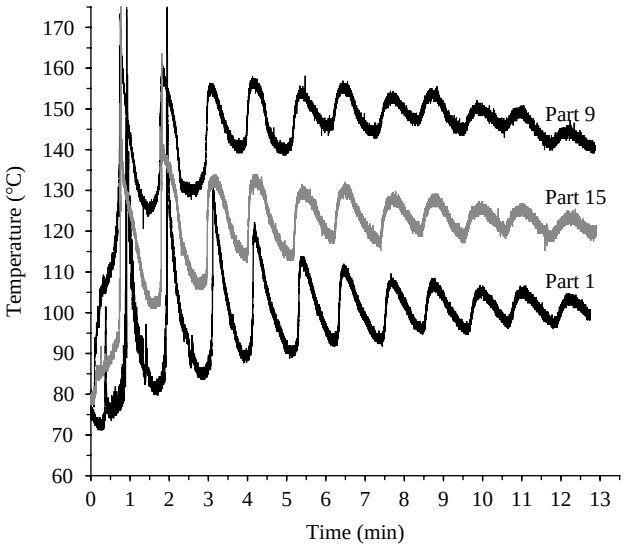

Table IV Effect of building location on mesostructure and mechanical properties

Part location	Part 1	Part 9	Part 15
Neck radius y (μm)	66.4	87.3	79.6
Standard deviation (μm)	4.82	4.42	3.63
Dimensionless neck growth (y/a)	0.54	0.71	0.65
Average failure load (N)	185.5	233.1	211.3
Standard deviation (N)	9.78	5.44	7.42

that the average temperature within the part is higher near the center building chamber (location 9) than the edge (location 1). This explains the large standard deviation in previous experiments. It also raises an important issue in future FDM process improvement and optimization.

Conclusions

Experiments were conducted to evaluate the effects of processing conditions on the quality of bonds achieved between adjacent filaments within a FDM part. The bond quality was experimentally assessed based on the growth of the neck formed between adjacent filaments and their failure under flexural loading. Experimental results showed that both the envelope temperature and variations in the convective conditions within the building chamber have strong effects on the mesostructure and the overall quality of the bond strength between filaments. Results suggest that better control of the cooling conditions may have strong repercussions on the mechanical properties and accuracy of the final part fabricated using the FDM process.

On-line measurements of the cooling temperature profiles of extruded filaments were carried out and used to assess the validity of models describing the FDM process. Our results showed that heat transfer models currently available in the literature are inadequate, as they either underestimate the heat transferred through conduction within the parts, or neglect variations in the convective conditions within the parts and during the fabrication process. The thermal history imposed on the material has important repercussions on the final mesostructure and bond strength achieved between polymer filaments. Under the conditions selected for the processing of ABS P400, the sintering phenomenon was found to have a significant effect on bond formation, but only for the very short duration when the filament's temperature was above the critical sintering temperature. Experimental evidence showed that the building material is exposed to temperatures above the glass transition, yet below the critical sintering temperature, for a large portion of the fabrication process. Under such conditions, creep deformation and molecular diffusion need to be considered in predicting the bond strength development and changes in the mesostructure.

References

Alexander, P. and Dutta, D. (2000), "Layered manufacturing of surfaces with open contours using localized wall thickening", *Computer Aided Design*, Vol. 32 No. 3, pp. 175-89.

Allen, S. and Dutta, D. (1998), "Wall thickness control in layered manufacturing for surfaces with closed slices", *Computational Geometry, Theory and Applications*, Vol. 10 No. 4, pp. 223-38.

Anitha, R., Arunachalam, S. and Radhakrishnan, P. (2001), "Critical parameters influencing the quality prototypes in fused deposition modelling", *Journal of Materials Processing Technology*, Vol. 118 Nos 1/3, pp. 385-8.

Bellehumeur, C.T., Bisaria, M.K. and Vlachopoulos, J. (1996), "An experimental study and model assessment of polymer sintering", *Polym. Eng. Sci.*, Vol. 36 No. 17, pp. 2198-207.

Bellehumeur, C., Li, L., Sun, Q. and Gu, P. (2004), "Modeling of bond formation between polymer filaments in the fused deposition modeling process", *Journal of Manufacturing Process*, Vol. 6 No. 2, pp. 170-8.

Bellini, A. (2002), "Fused deposition of ceramics: a comprehensive experimental, analytical and computational study of material behavior, fabrication process and equipment design", PhD thesis, Drexel University, Philadelphia, PA.

Comb, J.W., Priedeman, W.R. and Turley, P.W. (1994), "Layered manufacturing control parameters and material selection criteria", *Journal of Manufacturing Science and Engineering*, Vol. 68/2, pp. 547-56.

De Gennes, P.G. (1971), "Reptation of a polymer chain in the presence of fixed obstacles", *J. Chem. Phys.*, Vol. 55, pp. 572-9.

Gray, R.W., Baird, D.G. and Bohn, J.H. (1998), "Effects of processing conditions on short TLCP fiber reinforced FDM parts", *Rapid Prototyping Journal*, Vol. 4 No. 1, pp. 14-25.

Han, W.B., Jafari, M.A. and Seyed, K. (2003), "Process speeding up via deposition planning in fused deposition-based layered manufacturing processes", *Rapid Prototyping Journal*, Vol. 9 No. 4, pp. 212-8.

Kalita, S.J., Bose, S., Hosick, H.L. and Bandyopadhyay, A. (2003), "Development of controlled porosity polymer-ceramic composite scaffolds via fused deposition modeling", *Material Science and Engineering C*, Vol. 23 No. 5, pp. 611-20.

Kulkarni, P. and Dutta, D. (1999), "Deposition strategies and resulting part stiffness in layered manufacturing", *ASME Transactions: Journal of Manufacturing Science and Engineering*, Vol. 121 No. 1, pp. 93-103.

Li, L., Gu, P., Sun, Q. and Bellehumeur, C. (2003), "Modeling of bond formation in FDM process", *The Transactions of NAMRI/SME*, Vol. 31, pp. 613-20.

Li, L., Sun, Q., Bellehumeur, C. and Gu, P. (2002), "Composite modeling and analysis for fabrication of FDM prototypes with locally controlled properties", *Journal of Manufacturing Process*, Vol. 14 No. 2, pp. 129-32.

Luis Perez, C.J. (2002), "Analysis of the surface roughness and dimensional accuracy capability of fused deposition modelling processes", *International Journal of Production Research*, Vol. 40 No. 12, pp. 2865-81.

Narkis, M. (1979), "Sintering behavior of poly(methyl methacrylate) particles", *Polym. Eng. Sci.*, Vol. 19 No. 13, pp. 889-92.

Pandey, P.M., Reddy, N.V. and Dhande, S.G. (2003), "Improvement of surface finish by staircase machining in fused deposition modeling", *Journal of Materials Processing Technology*, Vol. 132 Nos 1/3, pp. 323-31.

Pokluda, O., Bellehumeur, C.T. and Vlachopoulos, J. (1997), "Modification of Frenkel's model for sintering", *AIChE Journal*, Vol. 43 No. 12, pp. 3253-6.

Rodríguez, J.F., Thomas, J.P. and Renaud, J.E. (2001), "Mechanical behavior of acrylonitrile butadiene styrene (ABS) fused deposition materials. Experimental investigation", *Rapid Prototyping Journal*, Vol. 7 No. 3, pp. 148-58.

Rodríguez, J.F., Thomas, J.P. and Renaud, J.E. (2003), "Mechanical behavior of acrylonitrile butadiene styrene fused deposition materials modeling", *Rapid Prototyping Journal*, Vol. 9 No. 4, pp. 219-30.

Rodríguez-Matas, J.F. (1999), "Modeling the mechanical behavior of fused deposition acrylonitrile-butadiene-styrene polymer components", PhD dissertation, Department of Aerospace and Mechanical Engineering, Notre Dame, IN.

Rosenzweig, N. and Narkis, M. (1981), "Sintering rheology of amorphous polymers", *Polym. Eng. Sci.*, Vol. 21 No. 17, pp. 1167-70.

Shofner, M.L., Lozano, K., Rodríguez-Macías, F.J. and Barrera, E.V. (2003), "Nanofiber-reinforced polymers prepared by fused deposition modeling", *Journal of Applied Polymer Science*, Vol. 89 No. 11, pp. 3081-90.

Sun, Q. (2005), "Bond formation between polymer filaments in fused deposition modeling process", MSc thesis, Department of Chemical and Petroleum Engineering, University of Calgary, Calgary.

Sung, H.A., Montero, M., Odell, D., Roundy, S. and Wright, P.K. (2002), "Anisotropic material properties of fused deposition modeling ABS", *Rapid Prototyping Journal*, Vol. 8 No. 4, pp. 248-57.

Thomas, J.P. and Rodríguez, J.F. (2000), "Modeling the fracture strength between fused deposition extruded roads", *Solid Freeform Fabrication Symposium Proceeding, Austin, TX, USA*.

Wang, F., Shor, L., Starly, B., Darling, A., Guceri, S. and Sun, W. (2003), "Fabrication of cellular polymer poly-(-caprolactone (PCL) scaffolds by precision extruding deposition process", *Bioengineering, Proceedings of the Northeast Conference*, pp. 181-2.

Wool, R.P. (1995), *Polymer Interface Structure and Strength*, Carl Hanser Verlag, New York, NY.

Yardimci, M.A. (1999), "Process analysis and planning for fused deposition", PhD dissertation, Department of Mechanical Engineering, University of Illinois, Chicago, IL.

Yardimci, M.A. and Guceri, S. (1996), "Conceptual framework for the thermal process modeling of fused deposition", *Rapid Prototyping Journal*, Vol. 2 No. 2, pp. 26-31.

Yardimci, M.A., Guceri, S., Danforth, S.C. and Agarwala, M. (1996), "Part quality prediction tools for fused deposition processing", *Proceedings of the Solid Freeform Fabrication Symposium, Austin, TX, USA*.

Zhong, W.H., Li, F., Zhang, Z.G., Song, L.L. and Li, Z. (2001), "Short fiber reinforced composites for fused deposition modeling", *Materials Science and Engineering*, Vol. A301, pp. 125-30.

Corresponding author

C.T. Bellehumeur can be contacted at: cbellehu@ucalgary.ca

This article has been cited by:

1. Jie Zhang, Xin Zhou Wang, Wang Wang Yu, Yu He Deng. 2017. Numerical investigation of the influence of process conditions on the temperature variation in fused deposition modeling. *Materials & Design* **130**, 59-68. [Crossref]
2. Wei Zhang, Amanda S. Wu, Jessica Sun, Zhenzhen Quan, Bohong Gu, Baozhong Sun, Chase Cotton, Dirk Heider, Tsu-Wei Chou. 2017. Characterization of residual stress and deformation in additively manufactured ABS polymer and composite specimens. *Composites Science and Technology* **150**, 102-110. [Crossref]
3. Carsten Koch, Luke Van Hulle, Natalie Rudolph. 2017. Investigation of mechanical anisotropy of the fused filament fabrication process via customized tool path generation. *Additive Manufacturing* **16**, 138-145. [Crossref]
4. C. McIlroy, P.D. Olmsted. 2017. Disentanglement effects on welding behaviour of polymer melts during the fused-filament-fabrication method for additive manufacturing. *Polymer* **123**, 376-391. [Crossref]
5. Anthony A. D'Amico, Analise Debaie, Amy M Peterson. Effect of layer thickness on irreversible thermal expansion and interlayer strength in fused deposition modeling. *Rapid Prototyping Journal* **0**:ja, 00-00. [Abstract] [PDF]
6. Xunfei Zhou, Sheng-Jen Hsieh, Yintong Sun. 2017. Experimental and numerical investigation of the thermal behaviour of polylactic acid during the fused deposition process. *Virtual and Physical Prototyping* **12**:3, 221-233. [Crossref]
7. S.F. Costa, F.M. Duarte, J.A. Covas. 2017. Estimation of filament temperature and adhesion development in fused deposition techniques. *Journal of Materials Processing Technology* **245**, 167-179. [Crossref]
8. Nahal Aliheidari, Rajasekhar Tripuraneni, Amir Ameli, Siva Nadimpalli. 2017. Fracture resistance measurement of fused deposition modeling 3D printed polymers. *Polymer Testing* **60**, 94-101. [Crossref]
9. Anselm Heuer, Pascal Pinter, Kay Andr? Weidenmann. 2017. Analysis of the Effects of Raster Orientation in Components Consisting of Short Glass Fibre Reinforced ABS of Different Fibre Volume Fraction Produced by Additive Manufacturing. *Key Engineering Materials* **742**, 482-489. [Crossref]
10. Douglas J. Gardner. Theories and Mechanisms of Adhesion in the Pharmaceutical, Biomedical and Dental Fields 1-21. [Crossref]
11. KhaliqMuhammad Hussam, Muhammad Hussam Khaliq, GomesRui, Rui Gomes, FernandesCélio, Célio Fernandes, NóbregaJoão, João Nóbrega, CarneiroOlga Sousa, Olga Sousa Carneiro, FerrásLuis Lima, Luis Lima Ferrás. 2017. On the use of high viscosity polymers in the fused filament fabrication process. *Rapid Prototyping Journal* **23**:4, 727-735. [Abstract] [Full Text] [PDF]
12. Maruti Hegde, Viswanath Meenakshisundaram, Nicholas Chartrain, Susheel Sekhar, Danesh Tafti, Christopher B. Williams, Timothy E. Long. 2017. 3D Printing All-Aromatic Polyimides using Mask-Projection Stereolithography: Processing the Nonprocessable. *Advanced Materials* **15**, 1701240. [Crossref]
13. Ethan Nyberg, Alexandra Rindone, Amir Dorafshar, Warren L. Grayson. 2017. Comparison of 3D-Printed Poly-ε-Caprolactone Scaffolds Functionalized with Tricalcium Phosphate, Hydroxyapatite, Bio-Oss, or Decellularized Bone Matrix . *Tissue Engineering Part A* **23**:11-12, 503-514. [Crossref]
14. Arno Ferreira, Khalid Mahmood Arif, Steven Dirven, Johan Potgieter. 2017. Retrofitment, open-sourcing, and characterisation of a legacy fused deposition modelling system. *The International Journal of Advanced Manufacturing Technology* **90**:9-12, 3357-3367. [Crossref]
15. Kam-Ming Mark Tam, Caitlin T. Mueller. 2017. Additive Manufacturing Along Principal Stress Lines. *3D Printing and Additive Manufacturing* **4**:2, 63-81. [Crossref]
16. R. Jerez-Mesa, G. Gomez-Gras, J.A. Travieso-Rodriguez, V. Garcia-Plana. 2017. A comparative study of the thermal behavior of three different 3D printer liquefiers. *Mechatronics* . [Crossref]
17. Charles B. Sweeney, Blake A. Lackey, Martin J. Pospisil, Thomas C. Achee, Victoria K. Hicks, Aaron G. Moran, Blake R. Teipel, Mohammad A. Saed, Micah J. Green. 2017. Welding of 3D-printed carbon nanotube?polymer composites by locally induced microwave heating. *Science Advances* **3**:6, e1700262. [Crossref]
18. Swayam Bikash Mishra, Rameez Malik, S. S. Mahapatra. 2017. Effect of External Perimeter on Flexural Strength of FDM Build Parts. *Arabian Journal for Science and Engineering* **169**. . [Crossref]
19. Lu Wang, Douglas J. Gardner, Douglas W. Bousfield. 2017. Cellulose nanofibril-reinforced polypropylene composites for material extrusion: Rheological properties. *Polymer Engineering & Science* **293**. . [Crossref]
20. Kevin R. Hart, Eric D. Wetzel. 2017. Fracture behavior of additively manufactured acrylonitrile butadiene styrene (ABS) materials. *Engineering Fracture Mechanics* **177**, 1-13. [Crossref]
21. Nagendra G. Tanikella, Ben Wittbrodt, Joshua M. Pearce. 2017. Tensile strength of commercial polymer materials for fused filament fabrication 3D printing. *Additive Manufacturing* **15**, 40-47. [Crossref]

22. CooganTimothy J., Timothy J. Coogan, KazmerDavid O., David O. Kazmer. 2017. Healing simulation for bond strength prediction of FDM. *Rapid Prototyping Journal* **23**:3, 551-561. [Abstract] [Full Text] [PDF]
23. Lu Wang, William M. Gramlich, Douglas J. Gardner. 2017. Improving the impact strength of Poly(lactic acid) (PLA) in fused layer modeling (FLM). *Polymer* **114**, 242-248. [Crossref]
24. R. J. Urbanic, R. W. Hedrick, C. G. Burford. 2017. A process planning framework and virtual representation for bead-based additive manufacturing processes. *The International Journal of Advanced Manufacturing Technology* **90**:1-4, 361-376. [Crossref]
25. AkandeStephen Oluwashola, Stephen Oluwashola Akande, DalgarnoKenny, Kenny Dalgarno, MunguiaJavier, Javier Munguia. 2017. Process control testing for fused filament fabrication. *Rapid Prototyping Journal* **23**:2, 246-256. [Abstract] [Full Text] [PDF]
26. CooganTimothy J., Timothy J. Coogan, KazmerDavid Owen, David Owen Kazmer. 2017. Bond and part strength in fused deposition modeling. *Rapid Prototyping Journal* **23**:2, 414-422. [Abstract] [Full Text] [PDF]
27. Soriano HerasEnrique, Enrique Soriano Heras, Blaya HaroFernando, Fernando Blaya Haro, de Agustín del BurgoJosé María, José María de Agustín del Burgo, Islán MarcosManuel Enrique, Manuel Enrique Islán Marcos. 2017. Plate auto-level system for fused deposition modelling (FDM) 3D printers. *Rapid Prototyping Journal* **23**:2, 401-413. [Abstract] [Full Text] [PDF]
28. TlegenovYedige, Yedige Tlegenov, WongYoke San, Yoke San Wong, HongGeok Soon, Geok Soon Hong. 2017. A dynamic model for nozzle clog monitoring in fused deposition modelling. *Rapid Prototyping Journal* **23**:2, 391-400. [Abstract] [Full Text] [PDF]
29. Charoula Kousiatza, Nikoleta Chatzidai, Dimitris Karalekas. 2017. Temperature Mapping of 3D Printed Polymer Plates: Experimental and Numerical Study. *Sensors* **17**:3, 456. [Crossref]
30. Claire McIlroy, Peter D. Olmsted. 2017. Deformation of an amorphous polymer during the fused-filament-fabrication method for additive manufacturing. *Journal of Rheology* **61**:2, 379-397. [Crossref]
31. Vidya Kishore, Christine Ajinjeru, Andrzej Nycz, Brian Post, John Lindahl, Vlastimil Kunc, Chad Duty. 2017. Infrared preheating to improve interlayer strength of big area additive manufacturing (BAAM) components. *Additive Manufacturing* **14**, 7-12. [Crossref]
32. Ashu Garg, Anirban Bhattacharya, Ajay Batish. 2017. Chemical vapor treatment of ABS parts built by FDM: Analysis of surface finish and mechanical strength. *The International Journal of Advanced Manufacturing Technology* **89**:5-8, 2175-2191. [Crossref]
33. Xinhua Liu, Mingshan Zhang, Shengpeng Li, Lei Si, Junquan Peng, Yuan Hu. 2017. Mechanical property parametric appraisal of fused deposition modeling parts based on the gray Taguchi method. *The International Journal of Advanced Manufacturing Technology* **89**:5-8, 2387-2397. [Crossref]
34. Shuna Meng, Hui He, Yunchao Jia, Peng Yu, Bai Huang, Jian Chen. 2017. Effect of nanoparticles on the mechanical properties of acrylonitrile-butadiene-styrene specimens fabricated by fused deposition modeling. *Journal of Applied Polymer Science* **134**:7. . [Crossref]
35. Xin Wang, Man Jiang, Zuowan Zhou, Jihua Gou, David Hui. 2017. 3D printing of polymer matrix composites: A review and prospective. *Composites Part B: Engineering* **110**, 442-458. [Crossref]
36. Yifan Jin, Yi Wan, Bing Zhang, Zhanqiang Liu. 2017. Modeling of the chemical finishing process for polylactic acid parts in fused deposition modeling and investigation of its tensile properties. *Journal of Materials Processing Technology* **240**, 233-239. [Crossref]
37. Lu Wang, Douglas J. Gardner. 2017. Effect of fused layer modeling (FLM) processing parameters on impact strength of cellular polypropylene. *Polymer* . [Crossref]
38. Fuda Ning, Weilong Cong, Yingbin Hu, Hui Wang. 2017. Additive manufacturing of carbon fiber-reinforced plastic composites using fused deposition modeling: Effects of process parameters on tensile properties. *Journal of Composite Materials* **51**:4, 451-462. [Crossref]
39. David Pollard, C. Ward, G. Herrmann, J. Etches. 2017. The manufacture of honeycomb cores using Fused Deposition Modeling. *Advanced Manufacturing: Polymer & Composites Science* **3**:1, 21-31. [Crossref]
40. N. Mohan, P. Senthil, S. Vinodh, N. Jayanth. 2017. A review on composite materials and process parameters optimisation for the fused deposition modelling process. *Virtual and Physical Prototyping* **12**:1, 47-59. [Crossref]
41. R.J. Zaldivar, D.B. Witkin, T. McLouth, D.N. Patel, K. Schmitt, J.P. Nokes. 2017. Influence of processing and orientation print effects on the mechanical and thermal behavior of 3D-Printed ULTEM® 9085 Material. *Additive Manufacturing* **13**, 71-80. [Crossref]
42. G. P. Tandon, T. J. Whitney, R. Gerzeski, H. Koerner, J. Baur. Process Parameter Effects on Interlaminar Fracture Toughness of FDM Printed Coupons 63-71. [Crossref]
43. Kshitiz Upadhyay, Ravi Dwivedi, Ankur Kumar Singh. Determination and Comparison of the Anisotropic Strengths of Fused Deposition Modeling P400 ABS 9-28. [Crossref]

44. Ala?aldin Alafaghani, Ala Qattawi, Muhammad Ali Ablat. 2017. Design Consideration for Additive Manufacturing: Fused Deposition Modelling. *Open Journal of Applied Sciences* **07**:06, 291-318. [Crossref]
45. Jung Hyun Park, Min-Young Lyu, Soon Yong Kwon, Hyung Jin Roh, Myung Sool Koo, Sung Hwan Cho. 2016. Temperature Analysis of Nozzle in a FDM Type 3D Printer Through Computer Simulation and Experiment. *Elastomers and Composites* **51**:4, 301-307. [Crossref]
46. Sofiane Guessasma, Sofiane Belhabib, Hedi Nouri, Omar Ben Hassana. 2016. Anisotropic damage inferred to 3D printed polymers using fused deposition modelling and subject to severe compression. *European Polymer Journal* **85**, 324-340. [Crossref]
47. K. G. Jaya Christiyan, U. Chandrasekhar, K. Venkateswarlu. 2016. Flexural Properties of PLA Components Under Various Test Condition Manufactured by 3D Printer. *Journal of The Institution of Engineers (India): Series C* . [Crossref]
48. S. Singh, R. Singh. 2016. Development of functionally graded material by fused deposition modelling assisted investment casting. *Journal of Manufacturing Processes* **24**, 38-45. [Crossref]
49. Jonathan E. Seppala, Kalman D. Migler. 2016. Infrared thermography of welding zones produced by polymer extrusion additive manufacturing. *Additive Manufacturing* **12**, 71-76. [Crossref]
50. Karla Monroy, Lidia Serenó, Joaquim De Ciurana Gay, Paulo Jorge Bártolo, Jorge Vicente Lopes Da Silva, Marco Domingos. Inkjet- and Extrusion-Based Technologies 121-160. [Crossref]
51. Miguel Fernandez-Vicente, Wilson Calle, Santiago Ferrandiz, Andres Conejero. 2016. Effect of Infill Parameters on Tensile Mechanical Behavior in Desktop 3D Printing. *3D Printing and Additive Manufacturing* **3**:3, 183-192. [Crossref]
52. Jenny Holländer, Natalja Genina, Harri Jukarainen, Mohammad Khajeheian, Ari Rosling, Ermei Mäkilä, Niklas Sandler. 2016. Three-Dimensional Printed PCL-Based Implantable Prototypes of Medical Devices for Controlled Drug Delivery. *Journal of Pharmaceutical Sciences* **105**:9, 2665-2676. [Crossref]
53. Jianlei Wang, Hongmei Xie, Zixiang Weng, T. Senthil, Lixin Wu. 2016. A novel approach to improve mechanical properties of parts fabricated by fused deposition modeling. *Materials & Design* **105**, 152-159. [Crossref]
54. Sebastian Hertle, Maximilian Drexler, Dietmar Drummer. 2016. Additive Manufacturing of Poly(propylene) by Means of Melt Extrusion. *Macromolecular Materials and Engineering* . [Crossref]
55. Xingchen Liu, Vadim Shapiro. 2016. Homogenization of material properties in additively manufactured structures. *Computer-Aided Design* **78**, 71-82. [Crossref]
56. Daniel P. Cole, Jaret C. Riddick, H. M. Iftekhar Jaim, Kenneth E. Strawhecker, Nicole E. Zander. 2016. Interfacial mechanical behavior of 3D printed ABS. *Journal of Applied Polymer Science* **133**:30. . [Crossref]
57. Leena Kumari Prasad, Hugh Smyth. 2016. 3D Printing technologies for drug delivery: a review. *Drug Development and Industrial Pharmacy* **42**:7, 1019-1031. [Crossref]
58. Rupinder Singh, Kanwalpreet Sahni. 2016. Some Investigations on Effect of Cooling Rate on Al2O3 Reinforced Al-MMC Prepared by Vacuum Moulding. *Journal of The Institution of Engineers (India): Series C* **97**:3, 431-435. [Crossref]
59. Sithiprumnea Dul, Luca Fambri, Alessandro Pegoretti. 2016. Fused deposition modelling with ABS–graphene nanocomposites. *Composites Part A: Applied Science and Manufacturing* **85**, 181-191. [Crossref]
60. R. Jerez-Mesa, J.A. Travieso-Rodriguez, X. Corbella, R. Busqué, G. Gomez-Gras. 2016. Finite element analysis of the thermal behavior of a RepRap 3D printer liquefier. *Mechatronics* **36**, 119-126. [Crossref]
61. Toby D. Brown, Paul D. Dalton, Dietmar W. Hutmacher. 2016. Melt electrospinning today: An opportune time for an emerging polymer process. *Progress in Polymer Science* **56**, 116-166. [Crossref]
62. Charoula Kousiatza, Dimitris Karalekas. 2016. In-situ monitoring of strain and temperature distributions during fused deposition modeling process. *Materials & Design* **97**, 400-406. [Crossref]
63. Singh Rupinder, Rupinder Singh, Singh Sunpreet, Sunpreet Singh, Mankotia Karan, Karan Mankotia. 2016. Development of ABS based wire as feedstock filament of FDM for industrial applications. *Rapid Prototyping Journal* **22**:2, 300-310. [Abstract] [Full Text] [PDF]
64. Zhiyuan Wang, Renwei Liu, Todd Sparks, Frank Liou. 2016. Large-Scale Deposition System by an Industrial Robot (I): Design of Fused Pellet Modeling System and Extrusion Process Analysis. *3D Printing and Additive Manufacturing* **3**:1, 39-47. [Crossref]
65. K.G. Jaya Christiyan, U. Chandrasekhar, K. Venkateswarlu. 2016. A study on the influence of process parameters on the Mechanical Properties of 3D printed ABS composite. *IOP Conference Series: Materials Science and Engineering* **114**, 012109. [Crossref]
66. Hongbin Li, Taiyong Wang, Jian Sun, Zhiqiang Yu. 2016. The adaptive slicing algorithm and its impact on the mechanical property and surface roughness of freeform extrusion parts. *Virtual and Physical Prototyping* **11**:1, 27-39. [Crossref]

67. O.A. Mohamed, S.H. Masood, J.L. Bhowmik. Optimisation of Dynamic Mechanical Thermal Properties of PC–ABS Parts Manufactured by FDM Process Using IV Optimal Design . [Crossref]
68. M. Faes, E. Ferraris, D. Moens. 2016. Influence of Inter-layer Cooling time on the Quasi-static Properties of ABS Components Produced via Fused Deposition Modelling. *Procedia CIRP* **42**, 748-753. [Crossref]
69. Vishal Francis, Prashant K. Jain. 2016. Experimental investigations on fused deposition modelling of polymer-layered silicate nanocomposite. *Virtual and Physical Prototyping* **11**:2, 109. [Crossref]
70. Ben Wittbrodt, Joshua M. Pearce. 2015. The effects of PLA color on material properties of 3-D printed components. *Additive Manufacturing* **8**, 110-116. [Crossref]
71. Miquel Domingo-Espin, Josep M. Puigoriol-Forcada, Andres-Amador Garcia-Granada, Jordi Llumà, Salvador Borros, Guillermo Reyes. 2015. Mechanical property characterization and simulation of fused deposition modeling Polycarbonate parts. *Materials & Design* **83**, 670-677. [Crossref]
72. Haixi Wu, Yan Wang, Zhonghua Yu. 2015. In situ monitoring of FDM machine condition via acoustic emission. *The International Journal of Advanced Manufacturing Technology* . [Crossref]
73. Wenzheng Wu, Peng Geng, Guiwei Li, Di Zhao, Haibo Zhang, Ji Zhao. 2015. Influence of Layer Thickness and Raster Angle on the Mechanical Properties of 3D-Printed PEEK and a Comparative Mechanical Study between PEEK and ABS. *Materials* **8**:9, 5834-5846. [Crossref]
74. Alberto Boschetto, Luana Bottini. 2015. Triangular mesh offset aiming to enhance Fused Deposition Modeling accuracy. *The International Journal of Advanced Manufacturing Technology* **80**:1-4, 99-111. [Crossref]
75. Quan Zhang, Dong Yan, Kai Zhang, Gengkai Hu. 2015. Pattern Transformation of Heat-Shrinkable Polymer by Three-Dimensional (3D) Printing Technique. *Scientific Reports* **5**:1. . [Crossref]
76. Bin Huang, Sarat B Singamneni. 2015. Curved Layer Adaptive Slicing (CLAS) for fused deposition modelling. *Rapid Prototyping Journal* **21**:4, 354-367. [Abstract] [Full Text] [PDF]
77. Stephen Oluwashola Akande, Kenny W. Dalgarno, Javier Munguia. 2015. Low-Cost QA Benchmark for Fused Filament Fabrication. *3D Printing and Additive Manufacturing* **2**:2, 78-84. [Crossref]
78. H. Rezayat, W. Zhou, A. Siriruk, D. Penumadu, S. S. Babu. 2015. Structure–mechanical property relationship in fused deposition modelling. *Materials Science and Technology* **31**:8, 895-903. [Crossref]
79. Sophia Ziemian, Maryvivian Okwara, Constance Wilkens Ziemian. 2015. Tensile and fatigue behavior of layered acrylonitrile butadiene styrene. *Rapid Prototyping Journal* **21**:3, 270-278. [Abstract] [Full Text] [PDF]
80. Brian N. Turner, Scott A Gold. 2015. A review of melt extrusion additive manufacturing processes: II. Materials, dimensional accuracy, and surface roughness. *Rapid Prototyping Journal* **21**:3, 250-261. [Abstract] [Full Text] [PDF]
81. Fengli Liu, Gursel Alici, Binbin Zhang, Stephen Beirne, Weihua Li. 2015. Fabrication and characterization of a magnetic micro-actuator based on deformable Fe-doped PDMS artificial cilium using 3D printing. *Smart Materials and Structures* **24**:3, 035015. [Crossref]
82. Pavan Kumar Gurrala, Srinivasa Prakash Regalla. 2014. Part strength evolution with bonding between filaments in fused deposition modelling. *Virtual and Physical Prototyping* **9**:3, 141-149. [Crossref]
83. Farzad Rayegani, Godfrey C. Onwubolu. 2014. Fused deposition modelling (FDM) process parameter prediction and optimization using group method for data handling (GMDH) and differential evolution (DE). *The International Journal of Advanced Manufacturing Technology* **73**:1-4, 509-519. [Crossref]
84. Brian N. Turner, Robert Strong, Scott A. Gold. 2014. A review of melt extrusion additive manufacturing processes: I. Process design and modeling. *Rapid Prototyping Journal* **20**:3, 192-204. [Abstract] [Full Text] [PDF]
85. Pavan Kumar Gurrala, Srinivasa Prakash Regalla. 2014. Multi-objective optimisation of strength and volumetric shrinkage of FDM parts. *Virtual and Physical Prototyping* **9**:2, 127-138. [Crossref]
86. S.H. Masood. Advances in Fused Deposition Modeling 69-91. [Crossref]
87. Antreas Kantaros, Dimitris Karalekas. 2013. Fiber Bragg grating based investigation of residual strains in ABS parts fabricated by fused deposition modeling process. *Materials & Design* **50**, 44-50. [Crossref]
88. Mario D. Monzón, Ian Gibson, Antonio N. Benítez, Luis Lorenzo, Pedro M. Hernández, María D. Marrero. 2013. Process and material behavior modeling for a new design of micro-additive fused deposition. *The International Journal of Advanced Manufacturing Technology* **67**:9-12, 2717-2726. [Crossref]
89. J. Martínez, J.L. Diéguez, E. Ares, A. Pereira, P. Hernández, J.A. Pérez. 2013. Comparative between FEM Models for FDM Parts and their Approach to a Real Mechanical Behaviour. *Procedia Engineering* **63**, 878-884. [Crossref]

90. Anoop K. Sood, Raj K. Ohdar, Siba S. Mahapatra. 2012. Experimental investigation and empirical modelling of FDM process for compressive strength improvement. *Journal of Advanced Research* **3**:1, 81-90. [Crossref]
91. Anoop Kumar Sood, Asif Equbal, Vijay Toppo, R.K. Ohdar, S.S. Mahapatra. 2012. An investigation on sliding wear of FDM built parts. *CIRP Journal of Manufacturing Science and Technology* **5**:1, 48-54. [Crossref]
92. A.W. Fatimatuzahraa, B. Farahaina, W.A.Y Yusoff. The effect of employing different raster orientations on the mechanical properties and microstructure of Fused Deposition Modeling parts 22-27. [Crossref]
93. A. Tsouknidas. 2011. Friction Induced Wear of Rapid Prototyping Generated Materials: A Review. *Advances in Tribology* **2011**, 1-7. [Crossref]
94. Nur Saaidah Abu Bakar, Mohd Rizal Alkahari, Hambali Boejang. 2010. Analysis on fused deposition modelling performance. *Journal of Zhejiang University-SCIENCE A* **11**:12, 972-977. [Crossref]
95. S.H. Choi, W.K. Zhu. 2010. A dynamic priority-based approach to concurrent toolpath planning for multi-material layered manufacturing. *Computer-Aided Design* **42**:12, 1095-1107. [Crossref]
96. A Equbal, A K Sood, V Toppo, R K Ohdar, S S Mahapatra. 2010. Prediction and analysis of sliding wear performance of fused deposition modelling-processed ABS plastic parts. *Proceedings of the Institution of Mechanical Engineers, Part J: Journal of Engineering Tribology* **224**:12, 1261-1271. [Crossref]
97. Anoop Kumar Sood, R.K. Ohdar, S.S. Mahapatra. 2010. Parametric appraisal of mechanical property of fused deposition modelling processed parts. *Materials & Design* **31**:1, 287-295. [Crossref]
98. Daekeon Ahn, Jin-Hwe Kweon, Soonman Kwon, Jungil Song, Seokhee Lee. 2009. Representation of surface roughness in fused deposition modeling. *Journal of Materials Processing Technology* **209**:15-16, 5593-5600. [Crossref]
99. Samir Kumar PANDA, Saumyakant PADHEE, Anoop Kumar SOOD, S. S. MAHAPATRA. 2009. Optimization of Fused Deposition Modelling (FDM) Process Parameters Using Bacterial Foraging Technique. *Intelligent Information Management* **01**:02, 89-97. [Crossref]